



# Green energy-efficient synthesis of Fe-ZSM-5 zeolite and its application for hydroxylation of phenol

Zeyu Han<sup>a</sup>, Feng Zhang<sup>b</sup>, Xinhong Zhao<sup>a,\*</sup>

<sup>a</sup> School of Petrochemical Engineering, Lanzhou University of Technology, Lanzhou, 730050, China

<sup>b</sup> Petrochina Yunnan Petrochemical Company Limited, Kunming, 650000, China

## ARTICLE INFO

### Keywords:

Solvent-free synthesis

Fe-ZSM-5

Fenton's reagent

Phenol hydroxylation

## ABSTRACT

Currently, there remains a great challenge to synthesize zeolites in an energy-saving and environmentally friendly manner. Herein we report a novel solvent-free route of synthesizing Fe-ZSM-5 zeolite, which is featured by using Fenton's reagent as a promoter. The influences of crystallization time, amount of hydrogen peroxide and low-temperature pretreatment on the synthesis of Fe-ZSM-5 zeolite were investigated in detail. The results indicate that the combination of solvent-free synthesis with Fenton's reagent can facilitate the rapid crystallization of Fe-ZSM-5 zeolite. The resultant Fe-ZSM-5 zeolite was used as a catalyst for phenol hydroxylation, and characterized by XRD, SEM, ICP-AES, N<sub>2</sub> physisorption and UV–Vis diffuse reflectance spectroscopy. Notably, it exhibits a much better catalytic performance as compared with the reference catalyst by conventional solvent-free method. The observed enhanced catalytic performance for this Fe-ZSM-5 catalyst is attributed to its larger BET surface area and mesoporous volume as well as enrichment towards phenol.

## 1. Introduction

Zeolites, as one of the most important porous materials in industry, have demonstrated their outstanding performances in various fields involving catalysis, adsorption, separation and ion exchange [1–7]. Conventional methods for synthesizing molecular sieves include such as hydrothermal, solvothermal and ionothermal method. These synthetic methods are usually carried out in the presence of solvent. However, the use of large amounts of solvent will inevitably lead to the generation of liquid wastes and/or high autogeneous pressure [8–10]. Recently, Xiao's group reported a novel route of synthesizing a series of zeolites without adding additional solvents, which was named as solvent-free synthesis. The absence of solvent, on the one hand, can avoid the generation of liquid wastes, and in the other hand, can completely eliminate the safety concerns related with high pressure. Owing to the “quasi-solid-solid conversion” mechanism of this novel solvent-free route [11], the utilization of raw materials was greatly improved, and the synthesis cost was thus significantly reduced [12–14]. However, it should be pointed out that the solvent-free synthesis of zeolites was usually performed under more harsh conditions, such as higher crystallization temperature and longer crystallization time, as compared to those solvent-mediated syntheses.

In recent years, with the increasing concern of energy crises around the world and continuous development of the concept of “green

chemistry”, there remains a great challenge to synthesize zeolites in an energy-saving and environmentally friendly manner. Most recently, Yu's group reported that hydroxyl free radicals from Fenton's reagent or UV irradiation can significantly accelerate the synthesis of zeolite [15]. It can be anticipated that the combination of solvent-free synthesis with hydroxyl free radicals may have the ability of simultaneously addressing the issues of serious pollution and high energy consumption from the preparation process of zeolites.

The direct hydroxylation of phenol with hydrogen peroxide over iron-based catalysts is a promising green catalytic process. Its main products, hydroquinone (HQ) and catechol (CAT), are indispensable raw materials or additives of producing dyes, perfumes, pharmaceuticals and rubber [16–21]. Fe-ZSM-5 was one of the most potential iron-based catalysts for phenol hydroxylation due to its unique three-dimensional pore structure (As shown in Fig. 1), adjustable acidity, shape selectivity and thermal stability. Several groups have reported the superior catalytic performances of Fe-ZSM-5 catalysts in this reaction [22–27]. However, the preparation process of these catalysts was relative complex and/or not environmentally benign.

In this work, we attempted to synthesize Fe-ZSM-5 zeolite with a solvent-free method promoted by Fenton's reagent. The influences of crystallization time, amount of hydrogen peroxide and low-temperature pretreatment on the synthesis of Fe-ZSM-5 zeolite were investigated in detail. The results indicated that Fe-ZSM-5 with high crystallinity could

\* Corresponding author.

E-mail address: [licpzhaohx@lut.cn](mailto:licpzhaohx@lut.cn) (X. Zhao).

<https://doi.org/10.1016/j.micromeso.2019.109679>

Received 17 May 2019; Received in revised form 31 July 2019; Accepted 23 August 2019

Available online 23 August 2019

1387-1811/ © 2019 Elsevier Inc. All rights reserved.

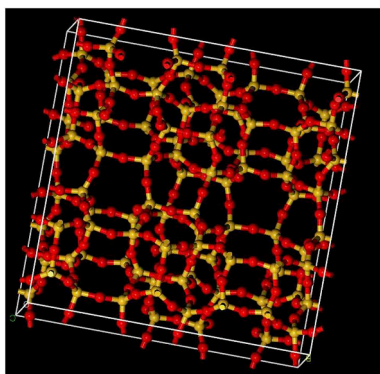


Fig. 1. Schematic diagram of the skeleton structure of ZSM-5 zeolite.

be synthesized in a shorter high-temperature crystallization time. Representative samples were selected as catalysts and tested in phenol hydroxylation reaction.

## 2. Experimental sections

### 2.1. Materials

$\text{Na}_2\text{SiO}_3 \cdot 9\text{H}_2\text{O}$  ( $\text{SiO}_2$  of 20 wt%, Tianjin Guangfu Chemical Reagent Co. Ltd), Fumed silica ( $\text{SiO}_2$  of 100 wt%, Aladdin Reagent), Tetrapropylammonium bromide (denoted as TPABr, 98%, Aladdin Reagent),  $\text{NH}_4\text{Cl}$  (Tianjin Fuchen Chemical Reagent Co. Ltd),  $\text{Fe}(\text{NO}_3)_3 \cdot 9\text{H}_2\text{O}$  (Tianjin Kaixin Chemical Industry Co. Ltd, China), hydrogen peroxide ( $\text{H}_2\text{O}_2$ , 30 wt% in water, Sinopharm Chemical Reagent Co. Ltd), phenol (Shanghai Guangnuo Chemical Technology Co. Ltd), ethanol (Li Anlong Bohua (Tianjin) Pharmaceutical Chemical Co. Ltd) and deionized water. All reagents were used without further purification.

### 2.2. Synthesis of Fe-ZSM-5

The process of preparing Fe-ZSM-5 zeolite: sodium silicate, fumed silica (0.33 g), TPABr, ammonium chloride and iron nitrate were added into a mortar one by one and mixed together [12]. The molar ratio of

the raw materials was 0.088: 1: 0.16: 1.345: 0.04 (If hydrogen peroxide was added to the reaction system, it would be added in a certain molar ratio of  $\text{H}_2\text{O}_2/\text{Fe}$ ), then the mixture was ground in a mortar for 15–20 min. The milled precursor mixture was transferred to a 25 ml Teflon-lined autoclave, which was then placed in a blast drying oven and crystallized at 180 °C for 18–72 h (or firstly pretreated at low temperature of 80 °C for 1–18 h before high-temperature crystallization). After the reaction was completed, the autoclave was rapidly cooled by flowing water and then thoroughly washed with deionized water and ethanol in order; the washed product was dried in a dry box at 110 °C for 150 min to obtain a solid raw powder product. The raw powder sample was calcined at 550 °C for 4 h to obtain a calcined powder. Final samples were designated as  $\text{HP}_x\text{-LT}_y\text{-HT}_z$ , where “HP”, “LT” and “HT” represent hydrogen peroxide, low temperature pretreatment and high temperature crystallization, respectively; x, y and z are the molar ratio of  $\text{H}_2\text{O}_2/\text{Fe}$ , pretreatment time at 80 °C and crystallization time at 180 °C, respectively. Detailed synthesis conditions and crystallinity data were listed in Table 1.

### 2.3. Characterization

X-ray diffraction (XRD) patterns were obtained on a D/Max-2400 Rigaku diffractometer with  $\text{Cu K}\alpha$  radiation operated at 40 kV and 150 mA. The crystallinities of the samples were calculated on the basis of the intensity of the peaks at  $2\theta$  of 23.09°, 23.33°, 23.72° and 23.96° and the following equation [28].

$$\text{Crystallinity}(\%) = \frac{\sum \text{intensity of XRD peaks of sample}}{\sum \text{intensity of XRD peaks of reference sample}} \times 100$$

Here the sample  $\text{HP}_0\text{-LT}_0\text{-HT}_{72}$  was used as the reference sample, whose crystallinity was defined as 100%. Scanning electron microscopic images (SEM) were collected by JSM 6701F instruments. Nitrogen adsorption/desorption studies were conducted on a Micromeritics ASAP 2020 surface area and pore size analyzer at −196 °C. Samples were outgassed at 350 °C for 4 h prior to the measurements. Specific surface areas of the specimens were calculated from the adsorption data obtained at  $p/p_0$  between 0.06 and 0.20, using the Brunauer–Emmett–Teller (BET) equation. The micropore volumes were determined by the t-plot method. The content of iron in the final product was quantified by IRIS Advantage Inductively Coupled Plasma-Atomic Emission Spectrometry (ICP-AES) measurement. Diffuse reflectance UV–Vis spectra (DR UV–Vis) were measured with a

Table 1  
Samples composition, crystallization conditions and crystallinity.

Samples <sup>a</sup>	$\text{Na}_2\text{SiO}_3 \cdot 9\text{H}_2\text{O}$ : fumed silica: TPABr: $\text{NH}_4\text{Cl}$ : $\text{Fe}(\text{NO}_3)_3 \cdot 9\text{H}_2\text{O}$ : $\text{H}_2\text{O}_2$	Crystallization conditions	Crystallinity % <sup>b</sup>
$\text{HP}_0\text{-LT}_0\text{-HT}_{18}$	0.088: 1: 0.16: 1.345: 0.04: 0	180 °C 18h	14
$\text{HP}_0\text{-LT}_0\text{-HT}_{24}$	0.088: 1: 0.16: 1.345: 0.04: 0	180 °C 24h	20
$\text{HP}_0\text{-LT}_0\text{-HT}_{36}$	0.088: 1: 0.16: 1.345: 0.04: 0	180 °C 36h	33
$\text{HP}_0\text{-LT}_0\text{-HT}_{48}$	0.088: 1: 0.16: 1.345: 0.04: 0	180 °C 48h	93
$\text{HP}_0\text{-LT}_0\text{-HT}_{72}$	0.088: 1: 0.16: 1.345: 0.04: 0	180 °C 72h	100
$\text{HP}_{2.5}\text{-LT}_{18}\text{-HT}_{24}$	0.088: 1: 0.16: 1.345: 0.04: 0.1	80 °C 18h + 180 °C 24h	56
$\text{HP}_0\text{-LT}_{18}\text{-HT}_{24}$	0.088: 1: 0.16: 1.345: 0.04: 0	80 °C 18h + 180 °C 24h	53
$\text{HP}_{2.5}\text{-LT}_0\text{-HT}_{24}$	0.088: 1: 0.16: 1.345: 0.04: 0.1	180 °C 24h	15
$\text{HP}_{0.5}\text{-LT}_{18}\text{-HT}_{24}$	0.088: 1: 0.16: 1.345: 0.04: 0.02	80 °C 18h + 180 °C 24h	67
$\text{HP}_{1.2}\text{-LT}_{18}\text{-HT}_{24}$	0.088: 1: 0.16: 1.345: 0.04: 0.048	80 °C 18h + 180 °C 24h	82
$\text{HP}_{4.0}\text{-LT}_{18}\text{-HT}_{24}$	0.088: 1: 0.16: 1.345: 0.04: 0.16	80 °C 18h + 180 °C 24h	53
$\text{HP}_{1.2}\text{-LT}_1\text{-HT}_{24}$	0.088: 1: 0.16: 1.345: 0.04: 0.048	80 °C 1h + 180 °C 24h	16
$\text{HP}_{1.2}\text{-LT}_3\text{-HT}_{24}$	0.088: 1: 0.16: 1.345: 0.04: 0.048	80 °C 3h + 180 °C 24h	29
$\text{HP}_{1.2}\text{-LT}_6\text{-HT}_{24}$	0.088: 1: 0.16: 1.345: 0.04: 0.048	80 °C 6h + 180 °C 24h	38
$\text{HP}_0\text{-LT}_6\text{-HT}_{24}$	0.088: 1: 0.16: 1.345: 0.04: 0	80 °C 6h + 180 °C 24h	32
$\text{HP}_0\text{-LT}_{12}\text{-HT}_{24}$	0.088: 1: 0.16: 1.345: 0.04: 0	80 °C 12h + 180 °C 24h	39
$\text{HP}_{1.2}\text{-LT}_{18}\text{-HT}_{28}$	0.088: 1: 0.16: 1.345: 0.04: 0.048	80 °C 18h + 180 °C 28h	203
$\text{HP}_{1.2}\text{-LT}_{18}\text{-HT}_{32}$	0.088: 1: 0.16: 1.345: 0.04: 0.048	80 °C 18h + 180 °C 32h	210
$\text{HP}_{1.2}\text{-LT}_{18}\text{-HT}_{36}$	0.088: 1: 0.16: 1.345: 0.04: 0.048	80 °C 18h + 180 °C 36h	263
$\text{HP}_{1.2}\text{-LT}_{18}\text{-HT}_{48}$	0.088: 1: 0.16: 1.345: 0.04: 0.048	80 °C 18h + 180 °C 36h	276

<sup>a</sup>  $\text{HP}_x\text{-LT}_y\text{-HT}_z$ , where “HP”, “LT” and “HT” represent hydrogen peroxide, low temperature pretreatment and high temperature crystallization, respectively; x, y and z are the molar ratio of  $\text{H}_2\text{O}_2/\text{Fe}$ , pretreatment time at 80 °C and crystallization time at 180 °C, respectively.

<sup>b</sup> Relative crystallinity: calculated with  $\text{HP}_0\text{-LT}_0\text{-HT}_{72}$  as 100%.

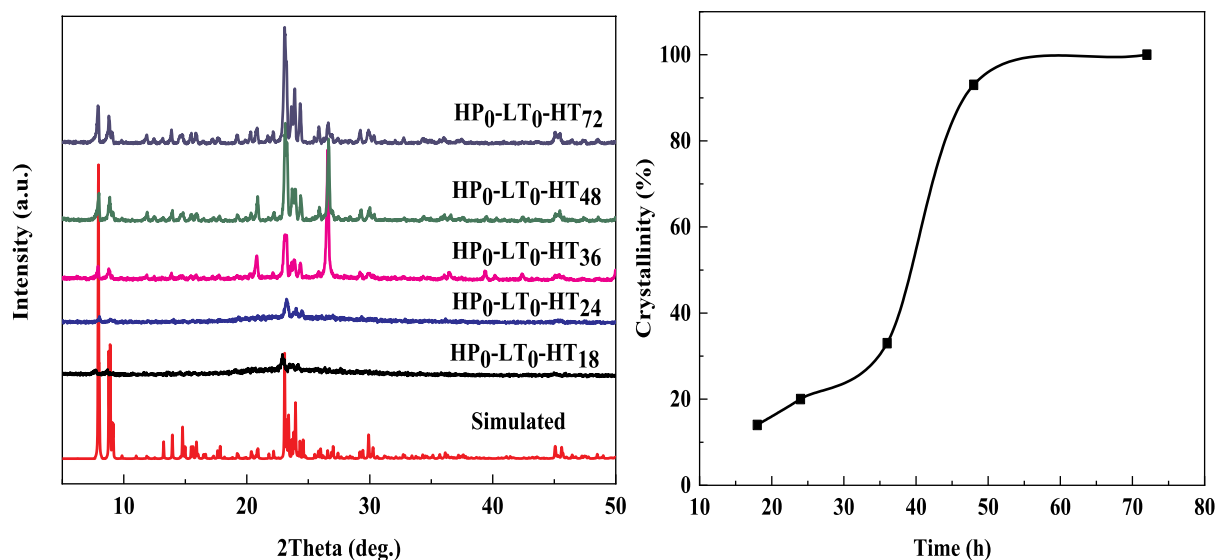


Fig. 2. XRD patterns and crystallization curve of Fe-ZSM-5 synthesized at different crystallization time.

spectrometer of Varian Gar 500, and BaSO<sub>4</sub> was an internal standard sample. UV/VIS spectrophotometer (7230G spectrophotometer, Shanghai precision scientific instrument Co. Ltd) was used to test the absorbance of phenol aqueous solution.

#### 2.4. Catalytic reaction

In a standard reaction, 2 g of phenol and 0.10 g of Fe-ZSM-5 catalyst were added to 24 mL of deionized water in a two-neck flask equipped with a magnetic stirrer and a reflux condenser. After heating the reaction mixture to 50 °C, 2.22 mL of hydrogen peroxide (H<sub>2</sub>O<sub>2</sub>, 30 wt% aqueous solution) was added through a syringe to the phenol solution containing catalyst (molar ratio of phenol/H<sub>2</sub>O<sub>2</sub> = 1/1). The product distributions were determined by a LC2000 HPLC (Tianmei, Shanghai, China) equipped with a reversed phase C18 column using the methanol/water mixture (40/60, volume ratio) as the mobile phase at the flow rate of 1.0 mL/min with UV detection at 277 nm.

The conversion of phenol (X%), the selectivity (S%) and the yield (Y%) of dihydroxybenzene can be calculated as follows:

$$X\% = \frac{n_{i0} - n_{i1}}{n_{i0}} \times 100\%$$

$$S\% = \frac{n_{i2}}{n_{i0} - n_{i1}} \times 100\%$$

$$Y\% = X\% \times S\%$$

In the above formula,  $n_{i0}$  and  $n_{i1}$  are the initial and final molar concentration of phenol, respectively;  $n_{i2}$  is the sum of molar concentration of formed hydroquinone and catechol after the reaction.

### 3. Results and discussion

#### 3.1. The crystallization curve of Fe-ZSM-5 without Fenton's reagent

Firstly, we synthesized a series of Fe-ZSM-5 samples according to Xiao's initial recipe [12]. The aim of this set of experiments was to search for the time that the crystallization of Fe-ZSM-5 was completed. Fig. 2 shows the XRD patterns and crystallization curve of the samples synthesized at five different crystallization times. The characteristic diffraction peaks attributed to MFI topology can be clearly observed from these patterns, indicating that Fe-ZSM-5 zeolites have been successfully synthesized. Furthermore, the diffraction patterns of these Fe-ZSM-5 samples are in agreement with those of simulated sample, confirming that these samples

are a pure MFI phase. As can be seen from the crystallization curve, the crystallinity of these Fe-ZSM-5 samples gradually increased with extended crystallization time. During the time range of 36 h–48 h, the crystallinity shows a maximum increasing rate of about 5%/hour. At 72 h, Fe-ZSM-5 has completely crystallized. Here the sample HP0-LT0-HT<sub>72</sub> was used as the reference sample, whose crystallinity was defined as 100%.

#### 3.2. The effect of Fenton's reagent

According to Yu's research, hydroxyl free radicals produced by Fenton's reagent can significantly enhance the crystallization rate of zeolites [15]. It is well known that H<sub>2</sub>O<sub>2</sub> undergoes self-decomposition at high temperature, while it is decomposed into •OH at the temperature of not higher than 80 °C. On the other hand, it was well known that the aging of amorphous gels at low temperature can increase the number of nuclei, which thus was in favor of shortening the induction time of zeolite synthesis and accelerating the crystallization process. In the following syntheses, several controlling experiments were conducted in order to make clear the individual effects of low-temperature pretreatment and Fenton's reagent on the crystallization rate of Fe-ZSM-5 zeolite.

Fig. 3 shows the XRD patterns of the samples synthesized under different crystallization conditions. The crystallinity of the sample

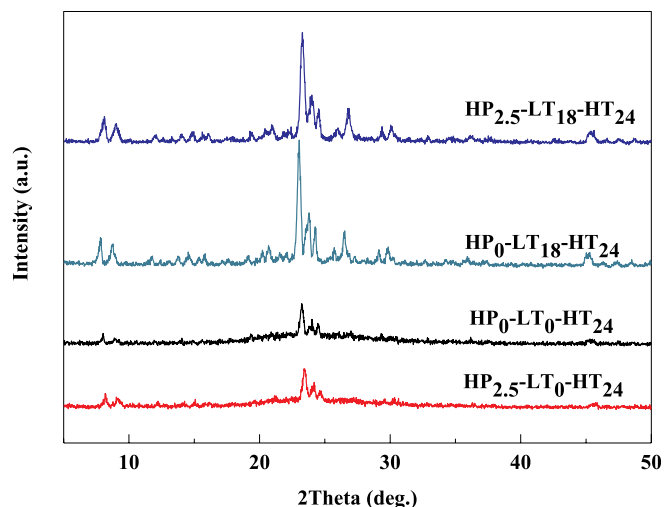


Fig. 3. XRD patterns of the samples synthesized under different situations.

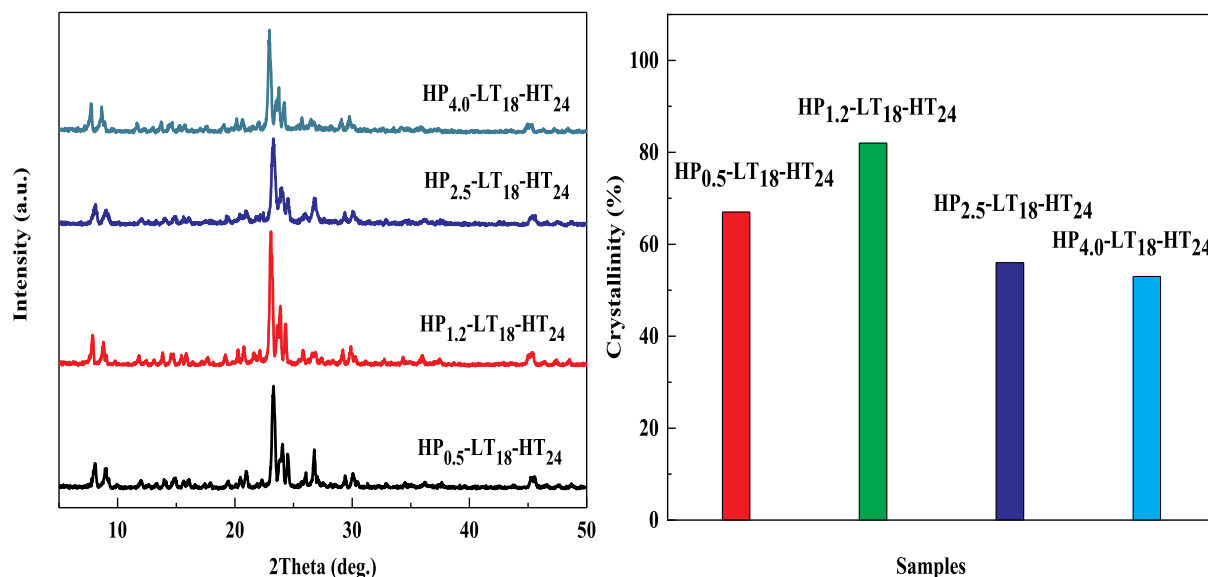


Fig. 4. XRD patterns and crystallization histogram of the samples synthesized with different amount of hydrogen peroxide.

HP<sub>2.5</sub>-LT<sub>18</sub>-HT<sub>24</sub>, HP<sub>0</sub>-LT<sub>18</sub>-HT<sub>24</sub>, and HP<sub>2.5</sub>-LT<sub>0</sub>-HT<sub>24</sub> was 56%, 53% and 15%, respectively. In comparison to HP<sub>0</sub>-LT<sub>0</sub>-HT<sub>24</sub>, the increased crystallinity for the sample HP<sub>0</sub>-LT<sub>18</sub>-HT<sub>24</sub> (20% vs. 53%) unambiguously indicates that the aging process of amorphous gels at the low temperature of 80 °C can enhance the crystallization of Fe-ZSM-5 [29]. As expected, the sample HP<sub>2.5</sub>-LT<sub>0</sub>-HT<sub>24</sub> shows a low crystallinity (15%), since no Fenton's reaction occurs in this synthesis. Unexpectedly, the sample HP<sub>2.5</sub>-LT<sub>18</sub>-HT<sub>24</sub> only exhibits a slightly higher crystallinity than the sample HP<sub>0</sub>-LT<sub>18</sub>-HT<sub>24</sub> (56% vs. 53%). The inappropriate amount of hydrogen peroxide added may be responsible for this result.

In the following study, a series of experiments were carried out to investigate the influence of the molar ratios of H<sub>2</sub>O<sub>2</sub>/Fe on the crystallinity, and the results are shown in Fig. 4. In the case where the molar ratio of H<sub>2</sub>O<sub>2</sub>/Fe was 0.5, 1.2, 2.5, and 4.0, the corresponding crystallinity of the samples was 67%, 82%, 56% and 53%, respectively. Obviously, the sample HP<sub>1.2</sub>-LT<sub>18</sub>-HT<sub>24</sub> reveals the highest crystallinity among these four samples. Peculiarly, its crystallinity is apparently higher than that of HP<sub>0</sub>-LT<sub>18</sub>-HT<sub>24</sub> (82% vs.

53%), demonstrating that Fenton's reagent can indeed enhance the crystallization rate of Fe-ZSM-5.

### 3.3. The effect of low-temperature pretreatment time

Since the purpose of this work is to increase the crystallinity of Fe-ZSM-5 zeolite in a shorter synthesis time, it is necessary to study the effect of pretreatment time on the crystallinity. Fig. 5 shows the XRD patterns and crystallization curve of the samples synthesized under the conditions of different low-temperature pretreatment time. The crystallinity of these samples almost linearly increases with extended pretreatment time. After linear regression, it is found that the slope of the crystallization curve is about 3.7%/hour. This increasing rate of crystallinity, however, should be considered as the contribution from both the low-temperature pretreatment and Fenton's reagent. The single contribution from low-temperature pretreatment reaches up to 1.8%/hour, which can be acquired from the slope of the crystallization curve in Fig. S1. After subtracting this rate of 1.8%/hour, the single contribution from Fenton's reagent is only 1.9%/hour. Nevertheless, the

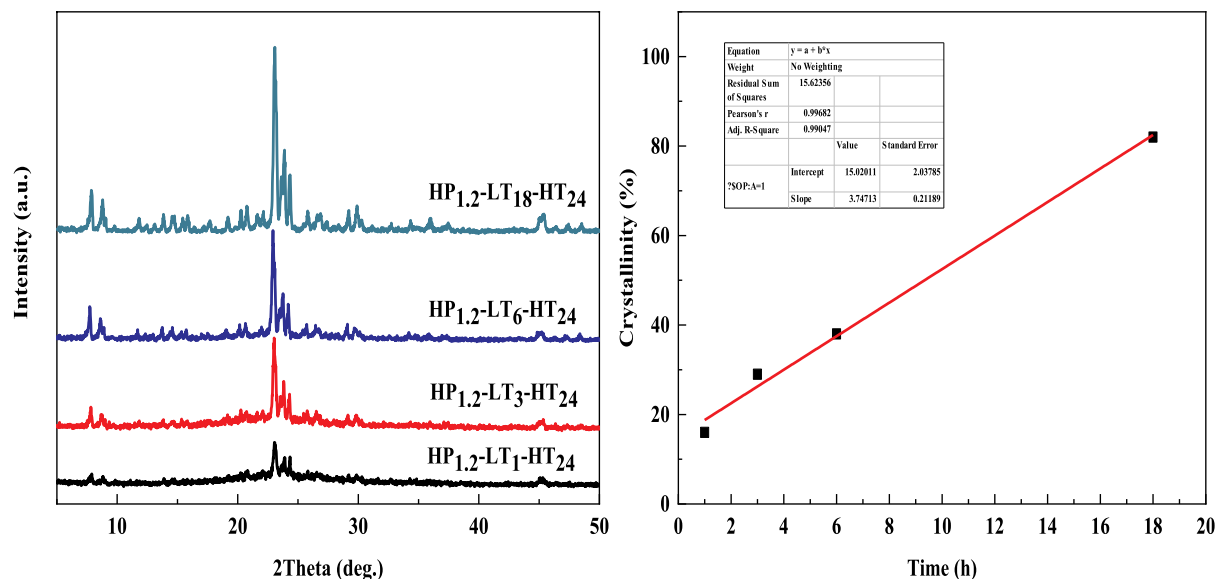


Fig. 5. XRD patterns and crystallization curve of the samples synthesized at different low-temperature pretreatment time.

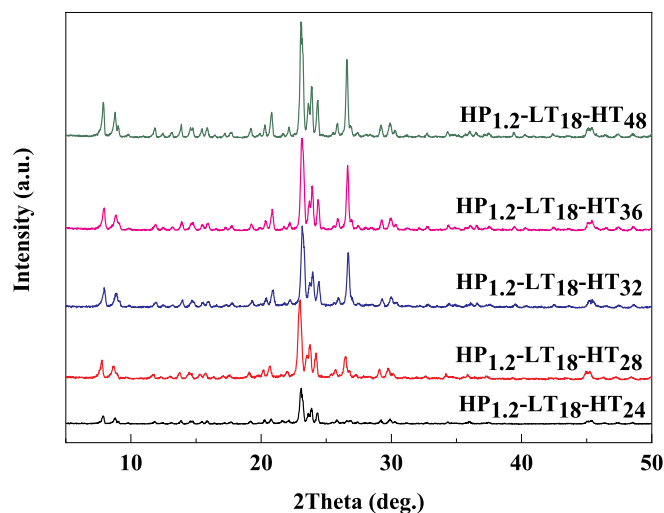


Fig. 6. XRD patterns of the samples synthesized at different high-temperature crystallization time.

combination of low-temperature pretreatment and Fenton's reagent can still be considered as a powerful tool of accelerating the crystallization rate of zeolites. However, from the point view of energy saving, it seems inappropriate to further increase the low-temperature pretreatment time.

#### 3.4. The effect of high-temperature crystallization time

It is well known that the crystallinity of zeolites is mainly determined by high-temperature crystallization time. As can be seen in Fig. 6 and Table 1, when the high-temperature crystallization time was prolonged from 24 h to 36 h and 48 h, the crystallinity of Fe-ZSM-5 abruptly increased from 82% to 263% and 276%, which were much higher than the reference sample  $\text{HP}_0\text{-LT}_0\text{-HT}_{72}$ . According to these data, it can be calculated that the high-temperature crystallization rate reaches the level of amazing 15%/hour during the time range of 24

h–36 h, which is three-fold higher than that without adding Fenton's reagent (5%/hour, see Section 3.1). These results fully demonstrate that the combination of low-temperature pretreatment with Fenton's reagent plays a key role in promoting the high-temperature crystallization of Fe-ZSM-5.

After a series of optimization, the suitable conditions for the synthesis of Fe-ZSM-5 zeolite with high crystallinity was obtained, and shown as follows: the initial molar composition of raw materials is  $\text{Na}_2\text{SiO}_3\cdot 9\text{H}_2\text{O}$ : fumed silica: TPABr:  $\text{NH}_4\text{Cl}$ :  $\text{Fe}(\text{NO}_3)_3\cdot 9\text{H}_2\text{O}$ :  $\text{H}_2\text{O}_2$  = 0.088: 1: 0.16: 1.345: 0.04: 0.048, the pretreatment time and high-temperature crystallization time are 18 h and 36 h, respectively. Although the total synthesis time (pretreatment time plus high-temperature crystallization time) for the sample  $\text{HP}_{1.2}\text{-LT}_{18}\text{-HT}_{36}$  is slightly longer compared with the sample  $\text{HP}_0\text{-LT}_0\text{-HT}_{48}$  (93% crystallinity), the former sample with extremely higher crystallinity is synthesized in a much shorter high-temperature crystallization time. Therefore, the synthetic strategy proposed here, i.e. the solvent-free synthesis promoted by Fenton's reagent, can be regarded as a green energy-efficient route of synthesizing iron-based zeolites.

#### 3.5. Morphology and pore texture analysis of Fe-ZSM-5

The SEM images of  $\text{HP}_0\text{-LT}_0\text{-HT}_{48}$  and  $\text{HP}_{1.2}\text{-LT}_{18}\text{-HT}_{36}$  are given in Fig. 7. The sample  $\text{HP}_0\text{-LT}_0\text{-HT}_{48}$  is composed of aggregates of spherical nanoparticles with size at about 100 nm. As a contrast, the sample  $\text{HP}_{1.2}\text{-LT}_{18}\text{-HT}_{36}$  consists of micron-sized crystals with length in the range of 5–10  $\mu\text{m}$ , verifying its high crystallinity. The other three samples with high crystallinity ( $\text{HP}_{1.2}\text{-LT}_{18}\text{-HT}_{24}$ ,  $\text{HP}_{1.2}\text{-LT}_{18}\text{-HT}_{28}$  and  $\text{HP}_{1.2}\text{-LT}_{18}\text{-HT}_{32}$ ) exhibit similar morphology to the sample  $\text{HP}_{1.2}\text{-LT}_{18}\text{-HT}_{36}$  (Fig. S2).

Fig. 8 shows  $\text{N}_2$  adsorption/desorption isotherms and pore size distribution curves of five representative samples. The specific structural parameters are listed in Table 2. As can be seen from the figure, the five samples feature the characteristic type-I adsorption isotherms, suggesting that both of them are typical microporous materials. Pronounced hysteresis loops appear at high relative pressure of the isotherms, indicating that the five samples contain a small number of additional mesopores or macropores. The data given in Table 2 also prove this result.

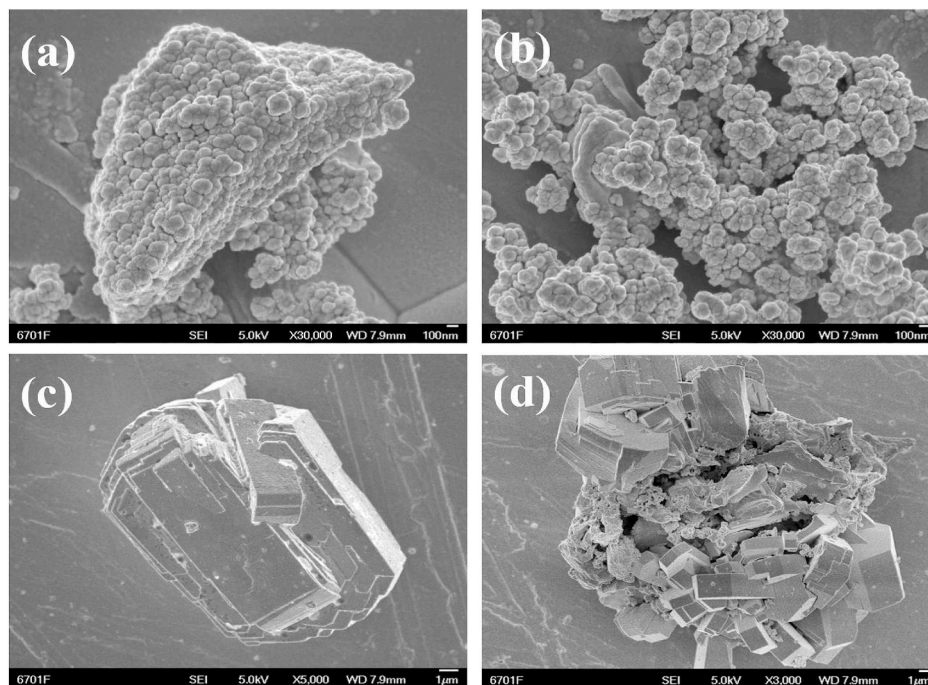


Fig. 7. SEM images of two representative Fe-ZSM-5 samples. (a) (b)  $\text{HP}_0\text{-LT}_0\text{-HT}_{48}$ ; (c) (d)  $\text{HP}_{1.2}\text{-LT}_{18}\text{-HT}_{36}$ .

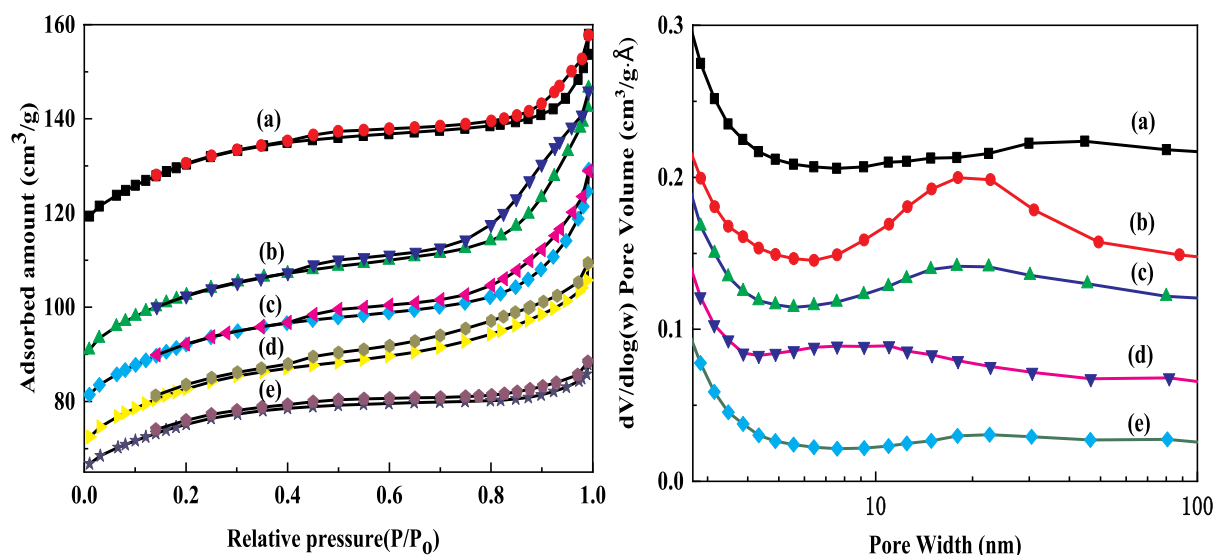


Fig. 8. N<sub>2</sub> adsorption/desorption isotherms and pore size distribution curves of five representative Fe-ZSM-5 samples. (a) HP<sub>1.2</sub>-LT<sub>18</sub>-HT<sub>24</sub>, (b) HP<sub>1.2</sub>-LT<sub>18</sub>-HT<sub>28</sub>, (c) HP<sub>1.2</sub>-LT<sub>18</sub>-HT<sub>32</sub>, (d) HP<sub>1.2</sub>-LT<sub>18</sub>-HT<sub>36</sub> and (e) HP<sub>0</sub>-LT<sub>0</sub>-HT<sub>48</sub>.

Table 2

Textural parameters of five representative Fe-ZSM-5 samples.

Sample	BET Surface area(m <sup>2</sup> /g)	Micropore Surface area(m <sup>2</sup> /g)	External Surface area(m <sup>2</sup> /g)	Micropore Volume (cm <sup>3</sup> /g) <sup>a</sup>	Mesopore Volume (cm <sup>3</sup> /g) <sup>b</sup>
HP <sub>1.2</sub> -LT <sub>18</sub> -HT <sub>24</sub>	302	205	97	0.095	0.078
HP <sub>1.2</sub> -LT <sub>18</sub> -HT <sub>28</sub>	300	205	95	0.095	0.105
HP <sub>1.2</sub> -LT <sub>18</sub> -HT <sub>32</sub>	275	181	94	0.084	0.093
HP <sub>1.2</sub> -LT <sub>18</sub> -HT <sub>36</sub>	282	193	89	0.090	0.074
HP <sub>0</sub> -LT <sub>0</sub> -HT <sub>48</sub>	254	180	75	0.083	0.046

<sup>a</sup> t-plot micropore volume.

<sup>b</sup> BJH adsorption cumulative volume of pores between 1.7 nm and 300 nm.

### 3.6. Phenol hydroxylation reaction over Fe-ZSM-5 catalysts

Iron-based zeolites are one kind of the most active catalysts for phenol hydroxylation. It was reported that iron-based zeolites such as Fe/HBEA [30], Fe-MCM-41 [31], Fe-HMS [32], FeAPO-5 [33] and Fe-MFI [26] have been used in the hydroxylation of phenol with hydrogen peroxide. In this work, two typical Fe-ZSM-5 catalysts were tested in this reaction. The corresponding catalytic results are summarized in Table 3. After 4 h reaction, HP<sub>1.2</sub>-LT<sub>18</sub>-HT<sub>36</sub> exhibits the best catalytic performance where the phenol conversion reaches about 40% and the

Table 3

Effect of reaction time on phenol hydroxylation over two Fe-ZSM-5 catalysts.

Catalyst	Time (h)	X <sub>ph</sub> (%) <sup>a</sup>	Y <sub>DHB</sub> (%) <sup>b</sup>	Product selectivity	
				(CAT + HQ) (%)	CAT/HQ
HP <sub>0</sub> -LT <sub>0</sub> -HT <sub>48</sub>	0.5	—	—	—	—
	1	—	—	—	—
	2	7.81	1.02	13.07	1.55
	3	7.69	1.59	20.67	1.53
	4	14.44	2.54	17.61	1.49
	5	14.13	3.19	22.58	1.44
HP <sub>1.2</sub> -LT <sub>18</sub> -HT <sub>36</sub>	6	12.44	3.77	30.32	1.49
	0.5	—	—	—	—
	1	—	—	—	—
	2	35.48	27.65	78.06	1.53
	3	39.06	31.17	79.88	1.58
	4	40.11	34.74	86.80	1.60
	5	44.00	34.88	80.08	1.63
	6	45.77	35.67	78.14	1.63

<sup>a</sup> X<sub>ph</sub> conversion of phenol.

<sup>b</sup> Y<sub>DHB</sub> yield of dihydroxybenzene.

selectivity of dihydroxybenzene is about 87%, whereas, for HP<sub>0</sub>-LT<sub>0</sub>-HT<sub>48</sub> the two indicators reflecting the catalytic performance are only 14% and 18%, respectively. This large difference between the two typical Fe-ZSM-5 catalysts should be attributed to their different structure and properties. Fe-ZSM-5 zeolites prepared by conventional solvent-mediated methods, were reported to show phenol conversion of ca. 38.4% and dihydroxybenzene selectivity of 84.2% in reference 25 [25], while in reference 27 phenol conversion of 42.3% with 92.5% selectivity to dihydroxybenzene was given [27]. Obviously, the catalytic performance of HP<sub>1.2</sub>-LT<sub>18</sub>-HT<sub>36</sub> is comparable to that of Fe-ZSM-5 catalysts prepared by conventional solvent-including methods.

To explain why this happened, a series of measurements including ICP-AES, UV-Vis diffuse reflectance spectra, adsorption capacity of catalysts towards phenol were conducted. The iron content of HP<sub>0</sub>-LT<sub>0</sub>-HT<sub>48</sub> and HP<sub>1.2</sub>-LT<sub>18</sub>-HT<sub>36</sub> determined by ICP-AES is 2.29 wt% and 2.06 wt%, respectively. The coordination environment of the iron species was studied by diffuse reflectance UV-Vis spectra [34,35], and the results are shown in Fig. 9. The absorption peaks at ca. 200 nm and 255 nm correspond to the isolated tetrahedral coordination Fe<sup>3+</sup>; the absorption peaks at ca. 315 nm and 378 nm are generally attributed to multinuclear Fe<sub>x</sub>O<sub>y</sub> located at the pores or the surface; and the Fe<sub>2</sub>O<sub>3</sub> nanoparticles on the zeolite surface mainly absorb at ca. 445 nm and 532 nm [36,37]. Obviously, three types of iron species are detected in both catalysts. As isolated tetrahedral coordination Fe<sup>3+</sup> are considered as the active center for phenol hydroxylation [32,38–40] and the sample HP<sub>0</sub>-LT<sub>0</sub>-HT<sub>48</sub> contains more isolated tetrahedral coordination Fe<sup>3+</sup> than HP<sub>1.2</sub>-LT<sub>18</sub>-HT<sub>36</sub>, the former catalyst should exhibit better catalytic performance than the latter. However, the observed catalytic results were reversed. Their different catalytic performance must be attributed to other reasons.

Except for iron species, the diffuse property of reactants and

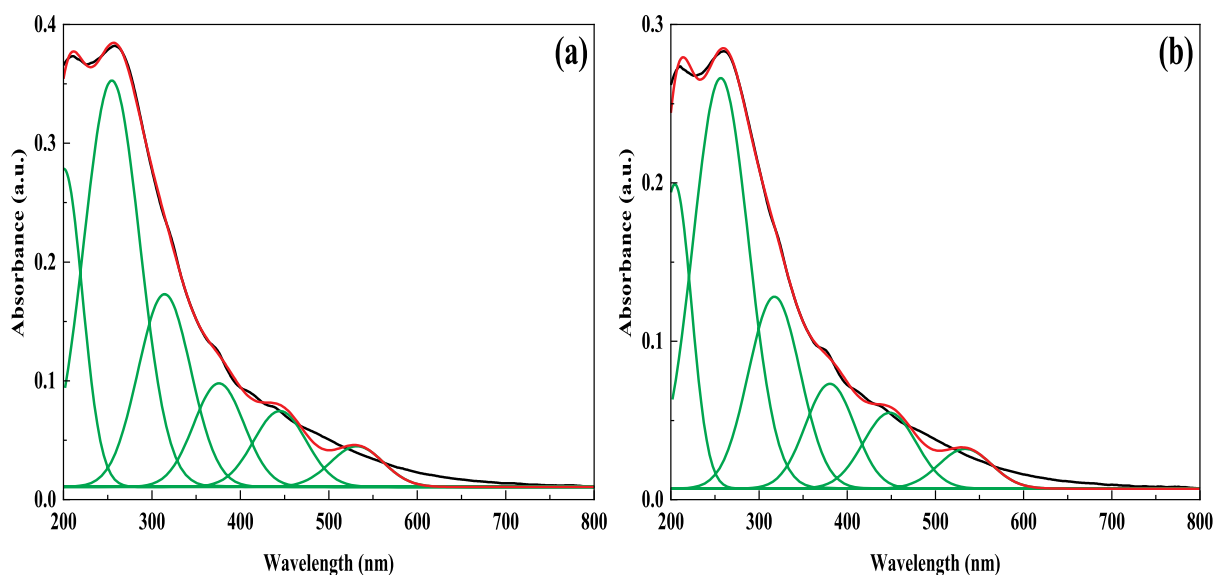


Fig. 9. UV-Vis diffuse reflectance spectra of two representative Fe-ZSM-5 samples. (a) HP<sub>0</sub>-LT<sub>0</sub>-HT<sub>48</sub>; (b) HP<sub>1.2</sub>-LT<sub>18</sub>-HT<sub>36</sub>.

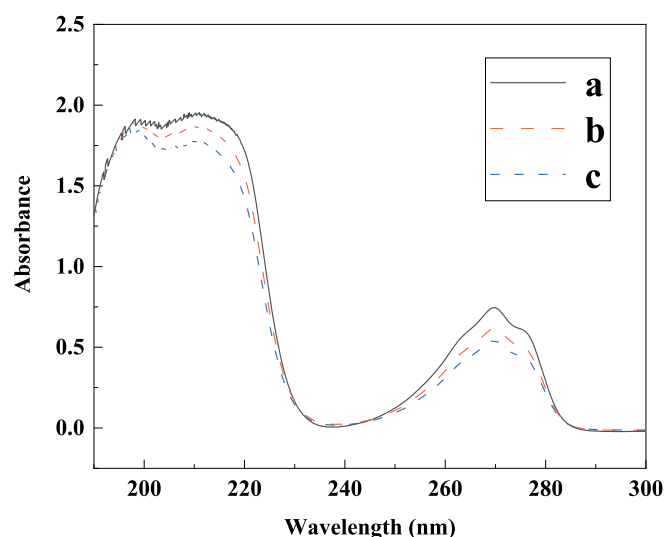


Fig. 10. UV-visible absorption spectrum of phenol solution: a: untreated phenol solution b: phenol solution treated by HP<sub>0</sub>-LT<sub>0</sub>-HT<sub>48</sub> c: phenol solution treated by HP<sub>1.2</sub>-LT<sub>18</sub>-HT<sub>36</sub>.

products in the narrow channels of Fe-ZSM-5 is another key factor of controlling its catalytic performance. For the sample HP<sub>1.2</sub>-LT<sub>18</sub>-HT<sub>36</sub>, its larger BET surface area and mesoporous volume as compared with HP<sub>0</sub>-LT<sub>0</sub>-HT<sub>48</sub> means that its active iron species are more easily accessible by reactants. On the other hand, the enhanced adsorption towards phenol on HP<sub>1.2</sub>-LT<sub>18</sub>-HT<sub>36</sub> may be also responsible for its excellent performance. As can be seen from Fig. 10, the phenol adsorption capacity of HP<sub>1.2</sub>-LT<sub>18</sub>-HT<sub>36</sub> is evidently higher than HP<sub>0</sub>-LT<sub>0</sub>-HT<sub>48</sub>, indicating that phenol is enriched on the former catalyst. The increased phenol concentration on the surface of catalyst is in favor of its subsequent fast conversion.

#### 4. Conclusions

In summary, a novel solvent-free route promoted by Fenton's reagent is designed to synthesize Fe-ZSM-5 zeolite with extremely high crystallinity in a shorter high-temperature crystallization time. The obtained material exhibits much better catalytic performance in the phenol hydroxylation reaction, when compared with the reference

catalyst by conventional solvent-free synthesis. The available data indicate that its excellent catalytic performance should be attributed to its larger BET surface area and mesoporous volume as well as enhanced adsorption towards phenol. Owing to the solvent-free feature and enhanced crystallization rate, the newly developed methodology of synthesizing Fe-ZSM-5 zeolite may find great potential applications in many other catalytic reactions with iron-based catalysts.

#### Acknowledgements

This work was supported by the National Natural Science Foundation of China (Grant No. 21666019) and the Natural Science Foundation of Gansu Province, China (Grant No.17JR5RA124).

#### Appendix A. Supplementary data

Supplementary data to this article can be found online at <https://doi.org/10.1016/j.micromeso.2019.109679>.

#### References

- [1] A.I. Lupulescu, J.D. Rimer, In situ imaging of silicalite-1 surface growth reveals the mechanism of crystallization, *Science* 344 (2014) 729–732 <https://doi.org/10.1126/science.1250984>.
- [2] A. Corma, V. Fornes, S.B. Pergher, M. Tlm, J.G. Buglass, Delaminated zeolite precursors as selective acidic catalysts, *Nature* 396 (1998) 353–356 <https://doi.org/10.1038/nature24592>.
- [3] P. Tung Cao Thanh, H.S. Kim, K.B. Yoon, Growth of uniformly oriented silica MFI and BEA zeolite films on substrates, *Science* 334 (2011) 1533–1538 <https://doi.org/10.1126/science.1212472>.
- [4] M.E. Davis, Ordered porous materials for emerging applications, *Nature* 417 (2002) 813–821 <https://doi.org/10.1038/nature00785>.
- [5] P.J. Bereciartua, A. Cantin, A. Corma, J.L. Jorda, M. Palomino, F. Rey, Control of zeolite framework flexibility and pore topology for separation of ethane and ethylene, *Science* 358 (2017) 1068–1071 <https://doi.org/10.1126/science.aao0092>.
- [6] M.Y. Jeon, D. Kim, P. Kumar, P.S. Lee, N. Rangnekar, P. Bai, M. Shete, B. Elyassi, H.S. Lee, K. Narasimharao, Ultra-selective high-flux membranes from directly synthesized zeolite nanosheets, *Nature* 543 (2017) 690 <https://doi.org/10.1038/nature21421>.
- [7] K. Shen, L. Zhang, X. Chen, L. Liu, D. Zhang, Y. Han, J. Chen, J. Long, R. Luque, Y. Li, Ordered macro-microporous metal-organic framework single crystals, *Science* 359 (2018) 206–210 <https://doi.org/10.1126/science.aao3403>.
- [8] D.M. Bibby, M.P. Dale, Synthesis of silica-sodalite from non-aqueous systems, *Nature* 317 (1985) 157–158 <https://doi.org/10.1038/317157a0>.
- [9] R.E. Morris, S.J. Weigel, The synthesis of molecular sieves from non-aqueous solvents, *Chem. Soc. Rev.* 26 (1997) 309–317 <https://doi.org/10.1039/CS9972600309>.
- [10] E.R. Cooper, C.D. Andrews, P.S. Wheatley, P.B. Webb, P. Wormald, R.E. Morris, Ionic liquids and eutectic mixtures as solvent and template in synthesis of zeolite

- analogues, *Nature* 430 (2004) 1012–1016 <https://doi.org/10.1038/nature02860>.
- [11] C. Zhang, S. Li, S. Bao, Sustainable synthesis of ZSM-5 zeolite from rice husk ash without addition of solvents, *Waste. Biomass. Valori* (2018) 1–11 <https://doi.org/10.1007/s12649-018-0356-0>.
  - [12] L. Ren, Q. Wu, C. Yang, L. Zhu, C. Li, P. Zhang, H. Zhang, X. Meng, F.-S. Xiao, Solvent-free synthesis of zeolites from solid raw materials, *J. Am. Chem. Soc.* 134 (2012) 15173–15176 <https://doi.org/10.1021/ja3044954>.
  - [13] Y. Jin, Q. Sun, G. Qi, C. Yang, J. Xu, F. Chen, X. Meng, F. Deng, F.-S. Xiao, Solvent-free synthesis of silicoaluminophosphate zeolites, *Angew. Chem. Int. Ed.* 52 (2013) 9172–9175 <https://doi.org/10.1002/anie.201302672>.
  - [14] N. Sheng, Y. Chu, S. Xing, Q. Wang, X. Yi, Z. Feng, X. Meng, X. Liu, F. Deng, F.-S. Xiao, Insights of the crystallization process of molecular sieve AlPO<sub>4</sub>-5 prepared by solvent-free synthesis, *J. Am. Chem. Soc.* 138 (2016) 6171–6176 <https://doi.org/10.1021/jacs.6b01200>.
  - [15] G. Feng, P. Cheng, W. Yan, M. Boronat, X. Li, J.H. Su, J. Wang, Y. Li, A. Corma, R. Xu, J. Yu, Accelerated crystallization of zeolites via hydroxyl free radicals, *Science* 351 (2016) 1188–1191 <https://doi.org/10.1126/science.aaf1559>.
  - [16] G.M. Rocha, R.A. Johnstone, M.G.P. Neves, Catalytic effects of metal (IV) phosphates on the oxidation of phenol and 2-naphthol, *J. Mol. Catal. A Chem.* 187 (2002) 95–104 [https://doi.org/10.1016/S1381-1169\(02\)00064](https://doi.org/10.1016/S1381-1169(02)00064).
  - [17] R. Klawekla, S. Kulprathipanja, P. Rangsunvigit, T. Rirksomboon, W. Rathbun, L. Nemeth, Kinetic modelling of phenol hydroxylation using titanium and tin silicate-1s: effect of tin incorporation, *Chem. Eng. J.* 129 (2007) 21–30 <https://doi.org/10.1016/j.cej.2006.10.034>.
  - [18] X. Zhao, Z. Sun, Z. Zhu, A. Li, G. Li, X. Wang, Evaluation of iron-containing aluminophosphate molecular sieve catalysts prepared by different methods for phenol hydroxylation, *Catal. Lett.* 143 (2013) 657–665 <https://doi.org/10.1007/s10562-013-1027-1>.
  - [19] S. Ikurumi, S. Okada, K. Nakatsuka, T. Kamegawa, K. Mori, H. Yamashita, Enhanced activity and selectivity in the one-pot hydroxylation of phenol by Pd/SiO<sub>2</sub>@ Fe-containing mesoporous silica core-shell catalyst, *J. Phys. Chem. C* 118 (2013) 575–581 <https://doi.org/10.1021/jp411153p>.
  - [20] F. Adam, J.-T. Wong, E.-P. Ng, Fast catalytic oxidation of phenol over iron modified zeolite L nanocrystals, *Chem. Eng. J.* 214 (2013) 63–67 <https://doi.org/10.1016/j.cej.2012.10.017>.
  - [21] I. Kuniarska-Biernacka, M.M.M. Raposo, R. Batista, P. Parpot, K. Biernacki, A.L. Magalhaes, A.M. Fonseca, I.C. Neves, Highly efficient heterogeneous catalysts for phenol oxidation: binuclear pyrrolyl-azine metal complexes encapsulated in NaY zeolite, *Microporous Mesoporous Mater.* 227 (2016) 272–280 <https://doi.org/10.1016/j.micromeso.2016.03.003>.
  - [22] A.L. Villa, C.A. Caro, C.M.d. Correa, Cu- and Fe-ZSM-5 as catalysts for phenol hydroxylation, *J. Mol. Catal. A Chem.* 228 (2005) 233–240 <https://doi.org/10.1016/j.molcata.2004.09.035>.
  - [23] S. Buttha, S. Youngme, J. Wittayakun, S. Loiha, Formation of iron active species on HZSM-5 catalysts by varying iron precursors for phenol hydroxylation, *Mol. Catal.* 461 (2018) 26–33 <https://doi.org/10.1016/j.mcat.2018.09.016>.
  - [24] L. Lang, X. Liu, M. Hu, B. Zhang, Highly enhanced phenol hydroxylation in [h0h]-Oriented Fe-ZSM-5 membranes, *ChemCatChem* 1 (2009) 472–478 <https://doi.org/10.1002/cctc.200900152>.
  - [25] J. Wang, J. Xu, B. Li, G. Zhang, N. Wu, L. Mao, Synthesis of a Fe-MFI zeolite with super-micropores by using potassium hexacyanoferrate(III) as an iron source, *Mater. Lett.* 124 (2014) 54–56 <https://doi.org/10.1016/j.matlet.2014.03.085>.
  - [26] A. Kessouri, B. Boukoussa, A. Bengueddach, R. Hamacha, Synthesis of iron-MFI zeolite and its photocatalytic application for hydroxylation of phenol, *Res. Chem. Intermed.* 44 (2018) 2475–2487 <https://doi.org/10.1007/s11164-017-3241-8>.
  - [27] Y. Shen, F. Wang, W. Liu, X. Zhang, The preparation of Fe<sup>3+</sup> ion-exchanged mesopore containing ZSM-5 molecular sieves and its high catalytic activity in the hydroxylation of phenol, *J. Porous Mater.* 25 (2018) 1587–1595 <https://doi.org/10.1007/s10934-018-0572-9>.
  - [28] P.W. Xu Ruren, Y.U. Jihong, *Molecular Sieve and Porous Materials Chemistry*, first ed., Science press, Beijing, 2004.
  - [29] K. Ding, A. Corma, J.A. Macia-Agullo, J.G. Hu, S. Kramer, P.C. Stair, G.D. Stucky, Constructing hierarchical porous zeolites via kinetic regulation, *J. Am. Chem. Soc.* 137 (2015) 11238–11241 <https://doi.org/10.1021/jacs.5b06791>.
  - [30] C. Kosri, K. Deekamwong, O. Sophiphun, N. Osakoo, N. Chanlek, K. Föttinger, J. Wittayakun, Comparison of Fe/HBEA catalysts from incipient wetness impregnation with various loading on phenol hydroxylation, *React. Kinet. Mech. Catal.* 121 (2017) 751–761 <https://doi.org/10.1007/s11444-017-1160-8>.
  - [31] J.S. Choi, S.S. Yoon, S.H. Jang, W.S. Ahn, Phenol hydroxylation using Fe-MCM-41 catalysts, *Catal. Today* 111 (2006) 280–287 <https://doi.org/10.1016/j.cattod.2005.10.037>.
  - [32] H. Liu, G. Lu, Y. Guo, Y. Guo, J. Wang, Study on the synthesis and the catalytic properties of Fe-HMS materials in the hydroxylation of phenol, *Microporous Mesoporous Mater.* 108 (2008) 56–64 <https://doi.org/10.1016/j.micromeso.2007.03.027>.
  - [33] X. Zhao, X. Zhang, Z. Hao, X. Gao, Z. Liu, Synthesis of FeAPO-5 molecular sieves with high iron contents via improved ionothermal method and their catalytic performances in phenol hydroxylation, *J. Porous Mater.* 25 (2018) 1007–1016 <https://doi.org/10.1007/s10934-017-0511-1>.
  - [34] B. Boukoussa, F. Abidallah, Z. Abid, Z. Talha, N. Taybi, H.S. El Hadj, Synthesis of polypyrrole/Fe-kanemite nanocomposite through in situ polymerization: effect of iron exchange, acid treatment, and CO<sub>2</sub> adsorption properties, *J. Mater. Sci.* 52 (2017) 2460–2472 <https://doi.org/10.1007/s10853-016-0541-0>.
  - [35] H. Sekkiou, B. Boukoussa, R. Ghezini, Z. Khenchoul, A. Ouali, R. Hamacha, A. Bengueddach, Enhanced hydrogen storage capacity of copper containing mesoporous silicas prepared using different methods, *Mater. Res. Express* 3 (2016) 085501 <https://doi.org/10.1088/2053-1591/3/8/085501>.
  - [36] L.D. Li, Q. Shen, J.J. Yu, Z.P. Hao, Z.P. Xu, G.Q.M. Lu, Fe-USY zeolite catalyst for effective decomposition of nitrous oxide, *Environ. Sci. Technol.* 41 (2007) 7901–7906 <https://doi.org/10.1021/es071779g>.
  - [37] M.S. Kumar, M. Schwidder, W. Grünert, A. Brückner, On the nature of different iron sites and their catalytic role in Fe-ZSM-5 DeNO<sub>x</sub> catalysts: new insights by a combined EPR and UV/VIS spectroscopic approach, *J. Catal.* 227 (2004) 384–397 <https://doi.org/10.1016/j.jcat.2004.08.003>.
  - [38] C. Wu, Y. Kong, F. Gao, Y. Wu, Y. Lu, J. Wang, L. Dong, Synthesis, characterization and catalytic performance for phenol hydroxylation of Fe-MCM41 with high iron content, *Microporous Mesoporous Mater.* 113 (2008) 163–170 <https://doi.org/10.1016/j.micromeso.2007.11.013>.
  - [39] H. Xin, J. Liu, F. Fan, Z. Feng, G. Jia, Q. Yang, C. Li, Mesoporous ferrosilicates with high content of isolated iron species synthesized in mild buffer solution and their catalytic application, *Microporous Mesoporous Mater.* 113 (2008) 231–239 <https://doi.org/10.1016/j.micromeso.2007.11.022>.
  - [40] B. Li, J. Xu, J. Liu, Z. Pan, Z. Wu, Z. Zhou, X. Pang, Preparation of mesoporous ferrisilicate: incorporation of iron onto mesoporous silica network by a novel route, *Mater. Lett.* 78 (2012) 147–149 <https://doi.org/10.1016/j.matlet.2012.03.034>.